

Experimental behaviour of composite beams subjected to a hogging moment

Marisa Pecce, Fernando Rossi*, Fabio Antonio Bibbò and Francesca Ceroni

Department of Engineering, University of Sannio, Italy

(Received August 24, 2010, Revised October 20, 2011, Accepted March 19, 2012)

Abstract. The present work addresses the rotational capacity of steel-concrete composite beams, which is a key issue for the seismic design of composite frames. Several experimental tests from the literature are summarised, and the effects of various parameters on the available plastic rotation are discussed. Furthermore, a number of remarks are made regarding the need for supplementary experimental results. The authors carried out experimental tests on four composite beams in which the type, width and connection degree of the slab were varied. During the tests, the deflection and strains in the steel profiles and bars were measured and recorded, wherein the observed trends in the measured parameters indicated that the failure mode of the beam was influenced by global and local buckling. A comparison of the experimental results to the theoretical ultimate strengths and moment-curvature relationships confirms that buckling phenomena occurred after section yielding, even if a consistent plastic rotation developed. This rotational capacity is well evaluated by a formulation that is available in the literature.

Keywords: rotational capacity; steel-concrete composite beams; composite frames; inelastic response; ductility.

1. Introduction

It has been well assessed in the technical literature and design codes that the performance of a structure under seismic actions largely depends on the deformation capacity of the components in the plastic region. In the case of reinforced concrete and steel structures, further studies are still in progress. Indeed, contemporary experimental results and the associated theoretical models have already identified the main mechanisms that govern nonlinear structural behaviour under monotonic and cyclic loads, and moreover, sophisticated and simplified models that are appropriate to research and practical design, respectively, are already available.

In the case of steel-concrete composite structures, numerous studies currently exist. Nevertheless, there is still a general lack of information regarding construction solutions that ensure high ductility. Additionally, design rules and modelling criteria (Eurocode 4 and Eurocode 8 2004) are still not complete or fully comprehensive, due to inherent difficulties that are especially related to the modelling of concrete behaviour in composite solutions and the interaction between steel and concrete components. In Italy, the growth and dissemination of technologies for composite structures, especially

* Corresponding author, Ph.D.student, E-mail: fernando@unisannio.it

for applications in seismic areas, are still limited, and specific standards (DM 14 January 2008) have been recently introduced. More generally, the use of moment-resisting frames consisting of composite elements is limited everywhere.

By broadly focusing on the influence of nonlinear behaviour on the performance of resisting frame structures, the modelling approach that features lumped plasticity appears particularly suitable for practical applications. This approach is based on well-assessed formulations of the available plastic rotation for reinforced concrete and steel members (Eurocode 3 and Eurocode 8 2004), and the results of joint modelling are available in the literature (El-Tawil *et al.* 1999). Unfortunately, the formulations that have been used to assess the rotational capacity of composite elements (beam, columns, joints) have still not been introduced in design codes, and often the performance of steel components is assumed in modelling composite structures (Providakis 2008).

Some models of steel-concrete composite frames have been developed by introducing distributed plasticisation along the members, as was investigated by Aribert *et al.* (2005) and Elghazouli *et al.* (2008).

The utility of assessing a local moment-rotation relationship is extensively addressed in Leon (1998) which underlines the importance of introducing the effects of the presence of an RC slab and partial connection.

An important contribution to understanding structural behaviour can be acquired by experimental tests on subcomponents because these tests are simple, economically convenient and are often more useful in focusing on a single parameter to calibrate numerical models in comparison to tests on entire, unscaled structures.

In fact, a number of experimental results are available regarding composite beams that have been tested with simple loading patterns to estimate the role of various components: the steel profile, slab, reinforcement and connection. In this case, the experimental test is usually carried out on a simple supported beam that has been loaded with a hogging moment by putting the slab in tension and the free flange of the profile in compression; this situation is the worst working condition for a steel-concrete composite beam. The results of other studies are reported in the next paragraph before the presentation and discussion of the new experimental results that have been developed by the authors. This simple type of experimental test has been chosen to provide information about the influence of the effective width, type of slab (with or without profiled sheet) and interaction level of the connection on the plastic rotation capacity of a beam; however, this experimental test neglects the effect of assembling the beam with the other components of a frame, such as the steel joint, transverse beam, hole in the slab and reinforcement details around the column.

In the opinion of the authors, further results concerning single members are still lacking, although they are necessary to assess the reliability of subcomponents, such as beams with plastic hinges at the edge, which are well calibrated with respect to composite behaviour and are necessary to develop a global model that is useful for practical nonlinear analysis. Moreover, this process of analysing subcomponents is very difficult based on the experimental results of the entire structure, where interaction phenomena are not negligible. The plastic rotational capacity of beams is particularly interesting because the global mechanism of moment-resisting frames can be determined if plastic hinges form in the beams rather than in other components (joints, columns).

2. Parameters influencing the rotational capacity

For composite beams, the rotational ductility in the hogging moment region depends on many factors: the concrete slab and its steel reinforcement, the shape of the steel profile and the shear connection devices (type, number and distribution). Furthermore, the effect of the beam-column joint must be introduced; in fact, there are some experimental programmes that have been developed (see, for example, Kemp and Nethercot 2001) to analyse and compare the different structural responses that are caused by the effect of beam-column semi-rigid joints, which contribute to local deformability and allow a greater rotational capacity with respect to rigid joints.

Collecting the results of some experimental programmes (Loh *et al.* 2004, Kemp *et al.* 1995, Fabbrocino *et al.* 2001, Amadio *et al.* 2004 and Nie *et al.* 2008) on simply supported beams that are subjected to negative bending, a brief summary of some fundamental parameters that govern the plastic rotational capacity therein has been carried out.

The following parameters have been selected as the most significant for the topic discussed in this study:

- the ratio $M_{pl} / M_{pl,a}$ between the plastic theoretical moment of the steel-concrete composite section and that of the steel profile, which represents the overstrength due to the composite action.
- the ratio $(A \cdot f_y)_r / (A \cdot f_y)_a$, which compares the resistance, i.e., the product of area and strength, of the steel bars (subscript r) to that of the profile (subscript a). This parameter is useful to identify the neutral axis position and, therefore, the part of the cross-section in compression that is used to estimate the local buckling of the profile.
- the ratio L / H_{tot} , which is a global parameter of the member slenderness, where L is the distance between the supports and H_{tot} the height of the composite section.
- the ratio $(f_t / f_y)_r$, which represents the overstrength of the reinforcement bars.
- the ratio between the ultimate and the yield strain of the steel bars $(\epsilon_u / \epsilon_y)_r$, which is an indicator of the reinforcement ductility.
- the ratio N / N_f , which represents the interaction degree of the shear connection.
- the parameter ρ , which is the geometric percentage of reinforcement in the slab.

In Table 1, for all of the collected experimental results, the values of the selected parameters are reported together with the experimental plastic rotation θ_{pl} ; the plastic rotation is measured by means of the rotation at the supports at 85% of the peak load on the descending branch of the load-displacement curve and cutting the rotation upon yielding. In the same table, the experimental results presented in this paper are listed, the details of which are provided in the following paragraphs.

The data shown in Table 1 do not allow for the clear identification of a direct relationship between each parameter and the plastic rotation because few results are available for each issue; nevertheless, some observations can be made.

Unfortunately, few data are available. It seems that the parameter ρ reduces the plastic rotation when it assumes excessively low or high values; this result is typical of RC elements in which great amounts of reinforcement reduce the yielding propagation of steel reinforcement, and small amounts can produce brittle failures during cracking. On the contrary, the overstrength $(f_t / f_y)_r$ does not seem to be a significant parameter for the examined composite beams because high values of this ratio have always been used. Regarding the effect of the partial shear connection, θ_{pl} decreases when the degree of the connection increases. Ultimately, an increase in the ratio $(\epsilon_u / \epsilon_y)_r$ implies, in general, an increment in the plastic deformation of the composite beams; however, it is no more influential when a certain value is exceeded.

Table 1 Values of θ_{pl} and parameters that influence the rotational capacity

Tests		Parameters							
		θ_{pl} (mrad)	P1	P2	P3	P4	P5	P6	P7
			$\frac{M_{pl}}{M_{pl,a}}$	$\frac{(A \cdot f_y)_r}{(A \cdot f_y)_a}$	L / H_{tot}	$(f_t / f_y)_r$	N / N_f	ρ (%)	$(\varepsilon_u / \varepsilon_y)_r$
Fabbrocino <i>et al.</i> (2001)	A1	164	1,27	0,14	12,03	1,16	1,00	0,64	70
	B1	145	1,27	0,14	12,03	1,16	1,00	0,64	70
Kemp <i>et al.</i> (1995)	MR2	3	1,30	0,17	8,98	-	1,00	0,31	10
	LR2	25	1,28	0,15	13,44	-	1,00	0,31	10
	SR	21	1,16	0,08	4,50	-	1,00	0,31	13
	LSR	49	1,37	0,26	13,56	-	1,00	0,50	4
	SSR	60	1,38	0,26	4,50	-	1,00	0,50	4
Loh <i>et al.</i> (2004)	CB1	31	1,99	0,35	6,79	1,27	0,83	1,95	85
	CB2	158	1,99	0,35	6,79	1,27	0,50	1,95	85
	CB3	152	1,99	0,35	6,79	1,27	0,33	1,95	85
	CB4	11	1,99	0,35	6,79	1,27	0,83	1,95	85
	CB5	64	1,99	0,35	6,79	1,27	0,50	1,95	85
	CB6	92	1,99	0,35	6,79	1,27	0,33	1,95	85
	CB7	166	1,48	0,17	6,79	1,27	1,00	0,98	85
	CB8	28	2,32	0,52	6,79	1,27	0,88	2,93	85
Amadio <i>et al.</i> (2004)	B1	87	1,45	0,18	12,67	1,29	1,00	1,00	10
	B2	110	1,45	0,18	12,67	1,29	1,00	1,00	10
Nie <i>et al.</i> (2008)	SB6	72	1,47	0,23	11,61	1,47	1,85	0,64	154
	SB7	67	1,66	0,36	11,61	1,47	1,16	1,03	154
	SB8	58	1,78	0,50	11,61	1,47	0,84	1,41	154
Pecce <i>et al.</i> (2009)	Beam 1	35	1,29	0,17	8,16	1,26	0,9	0,61	57
	Beam 2	41	1,29	0,17	8,16	1,26	1,3	0,61	57
	Beam 3	40	1,29	0,17	8,16	1,26	1,6	0,61	57
	Beam 4	45	1,42	0,28	8,16	1,26	1,1	0,60	57

The literature reveals some attempts to define simple rules that can be used to evaluate the rotational capacity of composite beams, but these formulations do not consider all of the parameters that have been introduced above. Among the available formulations, the following expression is proposed in Chen and Jia 2008:

$$\theta_u = \phi_{pl} \cdot l_p = \left(\frac{\varepsilon_{su}}{y_s} - \phi_e \right) \cdot l_p \quad (1)$$

Eq. (1) has a simple structure and expresses the product of the plastic curvature and the length of the plastic hinge (l_p), evaluating the plastic curvature as the difference between the ultimate curvature and the yielding curvature ($\phi_{pl} = \phi_u - \phi_e$). The ultimate curvature is evaluated as the ratio between the ultimate steel strain and the plastic neutral axis depth. The length of the plastic hinge has been

experimentally defined as being 1,75 times the total height of the composite section.

To evaluate the ultimate curvature, the following ultimate strain of the steel profile is proposed in the same paper (Chen and Jia 2008) to account for buckling:

$$\varepsilon_{su} = \frac{3000 \times 10^{-6}}{R + 0,05} \quad (2)$$

where $R = (A \cdot f_y)_r / (A \cdot f_y)_a$, which is a parameter that has already been introduced as an indicator of the profile depth in compression. Other values of ε_{su} can be used to consider the phenomenon of local buckling, as in the expression suggested by Kemp (1985), which summarises the contributions of various authors but is less safe than previous ones.

3. Experimental tests

3.1 Design features of the specimens

To obtain more information regarding the rotational capacity of composite beams subjected to hogging moments, three-point bending tests were carried out on four composite beams. A loading pattern with a concentrated force applied in the middle was developed to simulate the behaviour of the beam near the beam-column joint in a frame (Fig. 1). In fact, in a multi-story frame structure, in areas near the column, the beam is usually subjected to a hogging moment, which extends at least along one quarter of the span adjacent to the joint, due to vertical loads and along greater lengths, due to seismic actions. This simple supported pattern has been adopted by many researchers, as is the case in the aforementioned studies and results. Therefore, further restraints on global flexure-torsional buckling have not been applied because the constraint on the slab is usually considered sufficient; however, the test results show that global buckling occurs with torsional deformation together with local buckling, highlighting that distortional effects can occur in composite beams. This result is more extensively discussed later. To simplify the test procedure, the composite beam has been reversed by having the slab below and the steel profile above, obtaining the same working conditions for the materials as in the frame, i.e., tensile stresses in the slab and compression in the steel profile. The beams have a length of 4 m, which can be significant for a frame with spans ranging from 6 to 8 m. The steel profile is a double T with height = 360 mm, width = 170 mm, $t_w = 8$ mm and $t_f = 12,7$ mm. The thickness of the slab is 130 mm, which was constructed with and without profiled sheeting; in the latter case, two widths of the slab (1000 mm and 1600 mm) were realised.

The meaningful features of the beams are reported in Figs. 2, 3, and 4. The materials used in the

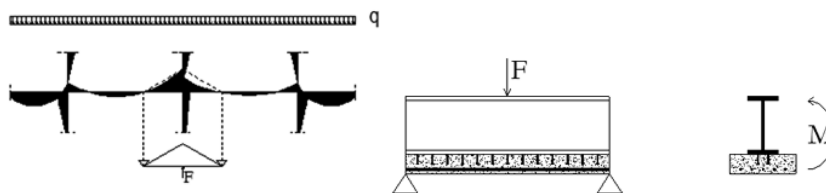


Fig. 1 Model of load used for the composite beams in the experiments

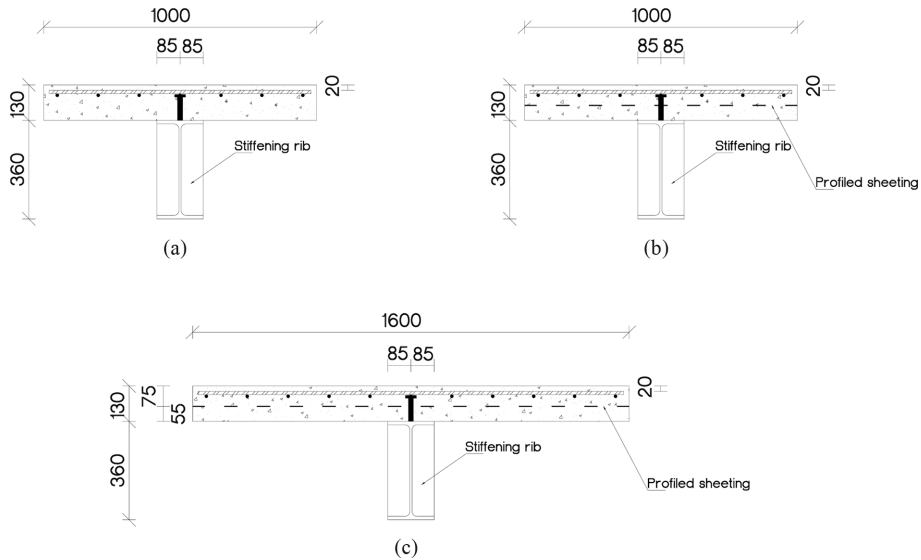


Fig. 2 Cross sections of the beams at mid-span [mm]: (a) Beams 1 and 2; (b) Beam 3 with a profiled sheeting; (c) Beam 4 with a profiled sheeting

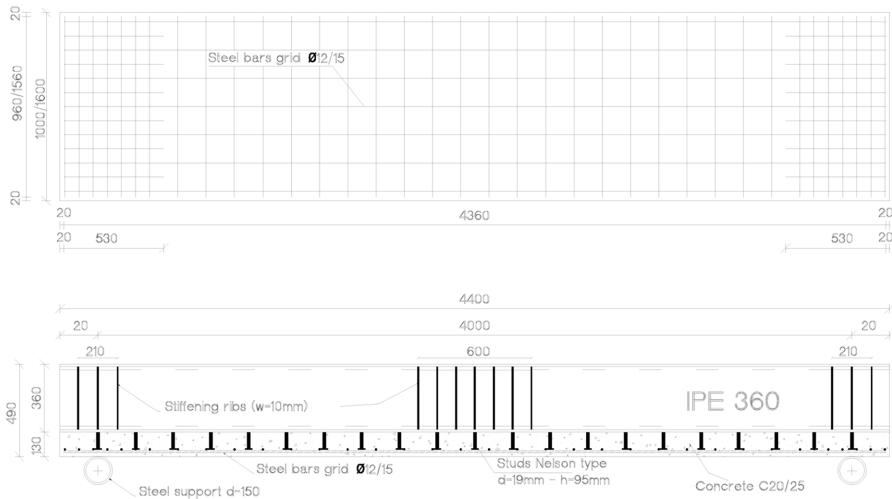


Fig. 3 Geometry of the beams [mm]

design are S275, B450C and C20/25 for the steel profile, steel bars and concrete, respectively, according to the European codification; the nominal characteristic yielding strength f_{yk} is 275 MPa and 450 MPa for constructional and reinforcing steel, respectively, and $f_{ck} = 20$ MPa is the nominal characteristic compressive strength of concrete. The classification of the sections according to Eurocode 4 was verified during the design process to estimate the slenderness of the flange and web and compare the results to code limits, as in the following.

For the flange, only the following verification is necessary:

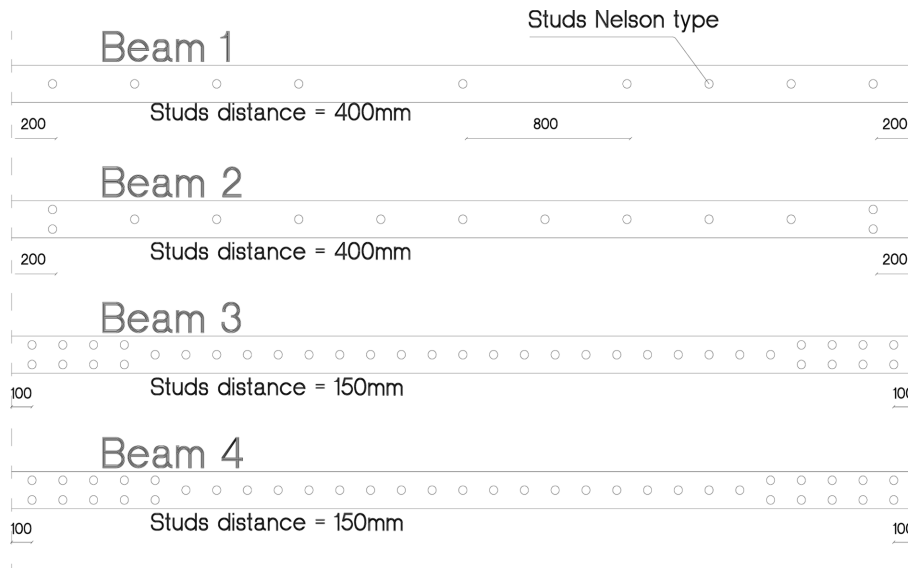


Fig. 4 Geometry of the connection [mm]



Fig. 5 Tested beams: slab with (on the left) and without (centre) profiled sheeting. Concrete cast of the slab (on the right)

$$\frac{c}{t_f} = \frac{85}{12,7} = 6,7 < 10 \cdot \varepsilon = 10 \cdot \sqrt{235/f_y} = 10 \sqrt{235/275} = 10 \cdot 0,92 = 9,2$$

⇒ Class 1 (compact section with high ductility)

For the web, the classification depends on the factor a , which is the rate of the web depth in compression; the extension of the web in compression depends on the amount and characteristics of the reinforcement bars in the slab because the profile is stressed by the bending moment and axial compression that is transmitted by the slab in tension, i.e., the slab reinforcement. Therefore, the neutral axis position where the plastic moment is attained has been evaluated by considering the nominal yield strength of the two steels, which is reduced by partial safety factors $\gamma_a = 1,1$ and $\gamma_s = 1,15$ for the profile and the reinforcement, respectively, and by neglecting the concrete tensile strength of the slab by taking into account only the contribution of reinforcement bars with 12-mm steel grid diameters (with a mesh of 150 mm, the steel area is 791 mm² in Beams 1, 2 and 3 and 1243 mm² in Beam 4).

The following results have been obtained:

Beam 1, 2 and 3

Neutral axis (web depth in compression) $x = 251$ mm

$$\alpha = \frac{x - (t_f + r)}{h - 2 \cdot (t_f + r)} = \frac{251,00 - (12,70 + 18,00)}{360,00 - 2 \cdot (12,70 + 18,00)} \Rightarrow 0,74 \Rightarrow \frac{d}{t_w} = 37,32 < \frac{393\varepsilon}{13\alpha - 1} \approx 42,61$$

\Rightarrow Class 1

where d is the clean height of the web regardless of the radius, r , at the web joint.

Beam 4

Neutral axis (web depth in compression) $x = 291$ mm

$$\alpha = \frac{x - (t_f + r)}{h - 2 \cdot (t_f + r)} = \frac{291,00 - (12,70 + 18,00)}{360,00 - 2 \cdot (12,70 + 18,00)} = 0,87 \Rightarrow \frac{d}{t_w} = 37,32 < \frac{456\varepsilon}{13\alpha - 1} \approx 40,79$$

\Rightarrow Class 2 (compact but with a limited ductility)

In conclusion, the cross-sections of Beams 1, 2 and 3 were designed in Class 1 and characterised by a high rotational capacity, and the cross-section of Beam 4 was designed in Class 2 due to the slenderness of the web rate in compression, which anticipates local buckling and, therefore, reduces the available ductility.

In the design of the specimens, further variability was applied to the degree of the connection and distribution of the connectors. The type of connection devices was fixed using a 19-mm diameter Nelson stud, which resulted in ductility for the geometry of the beams tested. The stud resistance was evaluated according to EC4 2004 and using all of the partial safety factors for the materials and the connectors; the resistance was determined to be 65,1 kN for beams with a full slab and 26,2 kN for beams with profiled steel sheeting. The number of studs that were required for the full interaction was

Table 2 Degree of connection of the beams

	Beam 1	Beam 2	Beam 3	Beam 4
$N_f = 2 \cdot \frac{F_{cf}}{f_{bd}}$	$2 \cdot \frac{295,77}{65,08} = 9,09 \cong 10$	$2 \cdot \frac{295,77}{65,08} = 9,09 \cong 10$	$2 \cdot \frac{295,77}{26,20} = 22,58 \cong 23$	$2 \cdot \frac{464,77}{26,20} = 35,48 \cong 36$
$\frac{N}{N_f}$	$\frac{9}{10} \cong 0,90$	$\frac{13}{10} \cong 1,30$	$\frac{37}{23} \cong 1,61$	$\frac{39}{36} \cong 1,09$

Table 3 Principal features of the composite beams used in experiments

ID Beams	Class	Connection type	Slab type	Effective width
Beam 1	1	Partial	Full slab	(1.0 m)
Beam 2	1	Full	Full slab	(1.0 m)
Beam 3	1	Full	Profiled sheeting	(1.0 m)
Beam 4	2	Full	Profiled sheeting	(1.6 m)

calculated by assuming that the ultimate tensile force of the rebars slab (F_{cf}) was to be transferred between the profile and slab, i.e., neglecting the contribution of the concrete to the tension. Table 2 depicts the number of connectors that were required for a full interaction together with the degree of connection for all of the specimens.

Therefore, only Beam 1 has a partial interaction together with a non-uniform distribution of connectors (Fig. 4) along the beam, and in fact, the studs were not applied in the middle part of the beam.

In Table 3, the meaningful characteristics of the specimens are summarised.

3.2 Experimental characterisation of the materials

To know the actual properties of the materials after beam construction, the steel and concrete that were experimentally used were characterised. Tensile tests were carried out on three specimens that were extracted from the web of the steel profile according to UNI 10002/92, resulting in the typical constitutive law depicted in Fig. 6 and the following average values

$$f_y = 401 \text{ MPa} \quad f_t = 588 \text{ MPa} \quad \varepsilon_{su} = 17,5\%$$

with standard deviations of 8,40 MPa, 8,80 MPa and 1,5%, respectively. According to the results, a characteristic value of $f_{yk} = 369 \text{ MPa}$ could be estimated.

Furthermore, for the reinforcing bars, three tensile tests were executed, thereby producing the following results as well as the typical constitutive relationship reported in Fig. 6

$$f_y = 455 \text{ MPa} \quad f_t = 577 \text{ MPa} \quad \varepsilon_u = 20,5\%$$

with standard deviations of 6,60 MPa, 3,60 MPa and 4,1%, respectively, from which a characteristic value of $f_{yk} = 430 \text{ MPa}$ could be estimated. The compression tests on three concrete cubes with 150-mm-long sides produced a mean value of 37,6 MPa.

In conclusion, the ratio of the actual characteristic value of the yield steel strength to the nominal one that was used in the design is approximately 1 for the steel reinforcement. Conversely, this ratio is equal

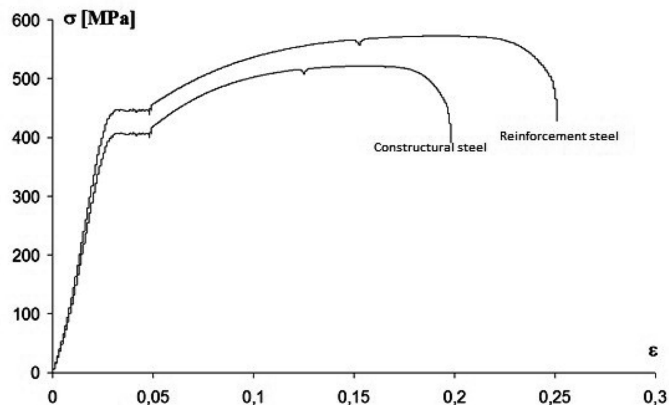


Fig. 6 Stress-strain relationship of the construction and bar steel

to 1,34 for constructional steel, which exceeds the limit of 1,20 set by Eurocodice 8 (the same in NTC 2008).

3.3 Evaluation of the actual characteristics of the beams

After the material tests suggested the relevant differences between the nominal and actual characteristics of the construction steel at yielding, the classification of the steel cross-section was revised using the actual yield strength of the steel profile and considering a unitary safety factor, which are better indicators of experimental behaviour than the design values.

The following are the classification results

- for the flanges

$$\frac{c}{t_f} = \frac{85}{12,7} = 6,7 < 10 \cdot \varepsilon = 10 \cdot \sqrt{235/f_y} = 10 \cdot \sqrt{235/369} = 10 \cdot 0,79 = 7,9 \Rightarrow \text{Class 1}$$

- for the webs:

Beam 1, 2 and 3

neutral axis (web height in compression) $x = 236$ mm

$$\alpha = \frac{x - (t_f + r)}{d} = \frac{236,00 - (12,70 + 18,00)}{360,00 - 2 \cdot (12,70 + 18,00)} = \frac{205,3}{298,6} = 0,69$$

$$\text{such that } \frac{d}{t_w} = 37,32 < \frac{393\varepsilon}{13\alpha - 1} \approx 38,18$$

Therefore, the profile remains in Class 1, albeit at the border line of Class 2 for the web slenderness.

Beam 4

neutral axis (web height in compression) $x = 268$ mm

$$\alpha = \frac{x - (t_f + r)}{d} = \frac{268,00 - (12,70 + 18,00)}{360,00 - 2 \cdot (12,70 + 18,00)} = \frac{237,3}{298,6} = 0,80$$

$$\text{such that } \frac{d}{t_w} = 37,32 < \frac{456\varepsilon}{13\alpha - 1} = 37,39$$

Therefore, the profile remains in Class 2, albeit at the border line of Class 3 for the web slenderness.

In conclusion, the actual yield strength of the steel profile formally does not change the classification of the section, even if the relationship between local slenderness and the limits of the code are significantly different from those used in the design.

For the connection degree, the actual transfer force between the slab and the steel profile is approximately the same as the designed one because the steel reinforcement has a yield strength that is close to that designed value; however, considering the actual value and assuming a unit safety factor for the connection, the connection degree of Beam 1 increases to 1, and the connection degrees of the other beams increase by about 10%.

3.4 Instrumentation

Several measuring instruments were placed on the tested specimens to identify the global and local behaviours of the beams during testing. The applied load and the deflection in the middle were respectively detected by a load cell and inductive transducer that were integrated into the jacket, which was used to load the beams by displacement control. Some strain gauges were glued along the height of the steel profile in two sections at 50 mm and 350 mm from the centre of the specimen because it was impossible to apply the instruments to the middle, where a stiffening rib had been welded. Before concrete casting, several strain gauges were placed on the reinforcing bars of the slab in the middle section of the beam, and others were placed at a distance of 300 mm from the centre.

Finally, some displacement transducers were arranged lengthwise to measure the horizontal slip between the steel beam and the concrete slab, and others were placed in the middle of the slab to monitor crack opening. In Fig. 7, the position of the strain gauges and the longitudinal transducers are reported.

3.5 Results

The yielding of the section was evidently reached, and plastic deformation developed. During the evolution of plasticisation, the phenomenon of local buckling in the compression region, flange and

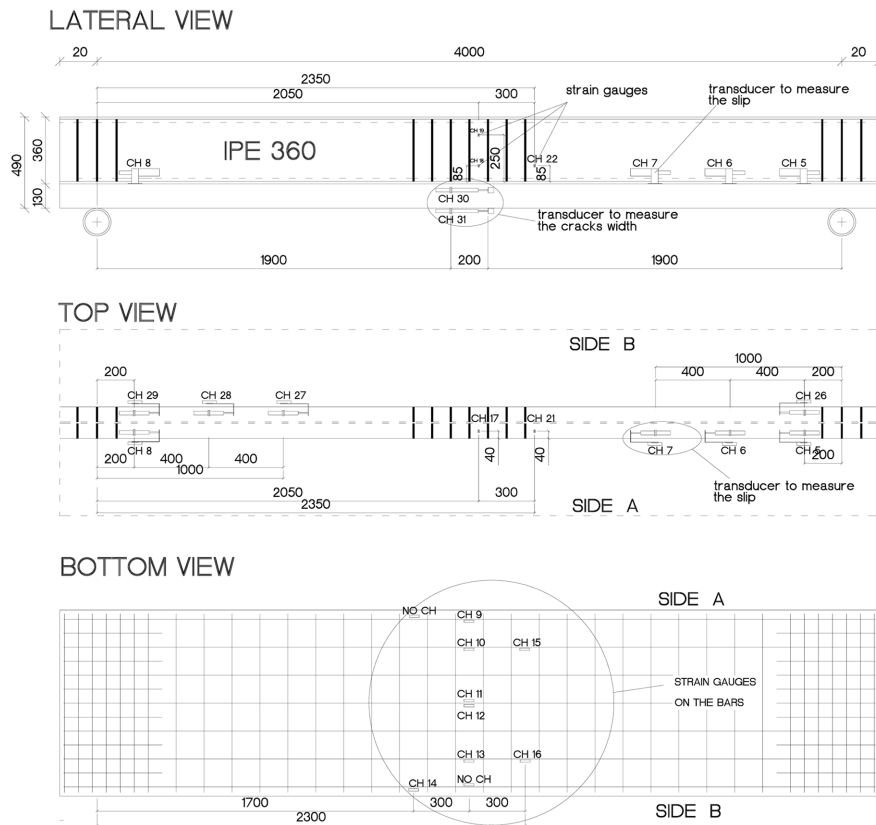


Fig. 7 Positions of the measuring instruments (all beams)

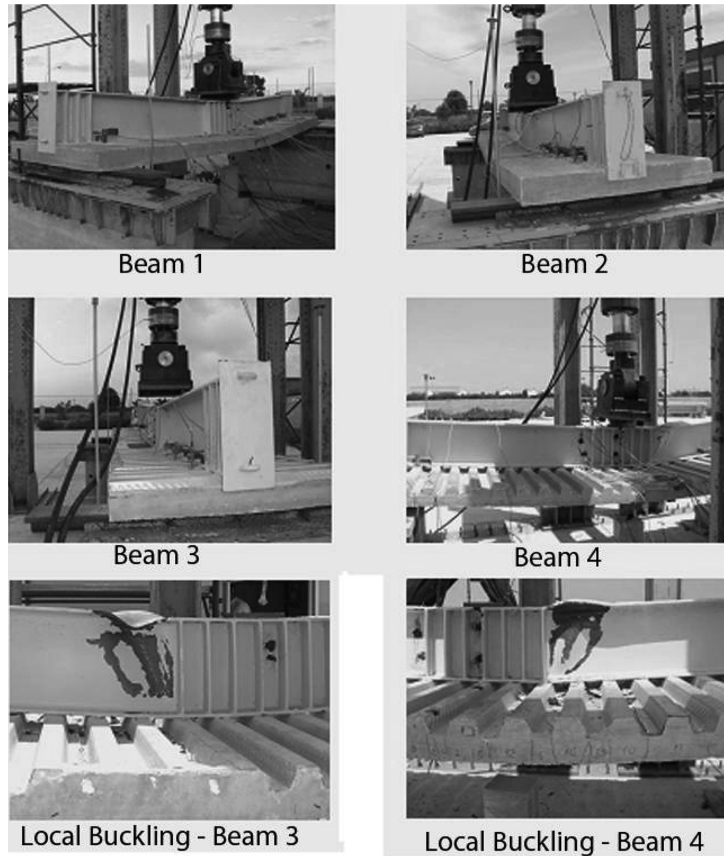


Fig. 8 Failure mode

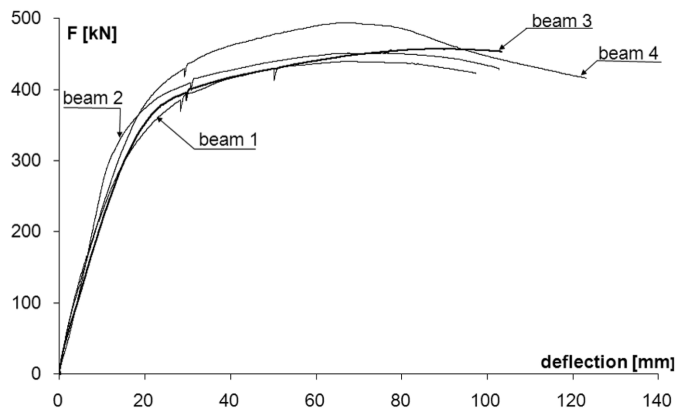


Fig. 9 Load-deflection curves for the four beams

part of the web, together with global torsional buckling, was observed.

Fig. 8 depicts photographs of the two phenomena. The test was stopped at a displacement of about 100 mm, when global and local buckling were evident, and for most of the beams, a reduction of the

load began.

As previously mentioned, the global buckling phenomenon was unexpected; therefore, the steel beam was not restrained for torsion.

Fig. 9 reports the load-deflection curves of the four beams; after a similar beginning branch before concrete cracking, several differences are evident, especially those due to the variation of the connection or type of RC slab. A comparison between Beams 1 and 2 reveals a reduction in the strength and stiffness of Beam 1, where the connection degree is lower than 1 and there are no studs in the central part of the beam; however, the peak moment occurs at the same displacement for both beams, and the descending branch exhibits the same trend. Beam 2 is similar to Beam 3 in that it has a full connection, and the slab has a width of 1000 mm; however, the slab is realised with profiled sheeting. Beam 3 shows a lower stiffness than Beam 2, probably due to the lower efficiency of the connection when the profiled sheeting is used; however, the maximum moment is slightly higher, probably due to the contribution of the profiled sheeting. Furthermore, the descending branch begins at a greater displacement, approximately when the test was stopped. Finally, Beam 3 differs from Beam 4 with respect to its greater slab width. The maximum moment increases in Beam 4 due to the larger amount of slab reinforcement, which indicates that the slab width is effective. This increase in strength follows a steeper descending branch, due to the higher sensitivity of this section to the local buckling of the web, which has a longer part in compression, as is already known from the classification (Beam 4 is in Class 2, Beam 3 is in Class 1).

To estimate the plastic rotational capacity, the following rotations have been evaluated

- θ_y , corresponding to the load when the yielding moment M_y is reached.
- θ_u , at 85% of the maximum load ($F_{0,85}$) taken on the descending branch of the load-deflection curve, as was already done for the results discussed in paragraph 2. In actuality, the tests were stopped before the development of the descending branch reached this level of decrement, so the conditions coincide with those of the last measured load.
- θ_{max} at the maximum load.

All of the rotations have been estimated by dividing the deflection at the corresponding load by the half-length of the beams, the results of which are summarised in Table 4. The yielding moment of the composite section has been computed by assuming a full interaction and using the actual characteristics of the materials, wherein it follows that the yielding of the cross-section implies the yielding of the reinforcement for Beams 1, 2 and 3 in addition to the yielding of the constructional steel in compression for Beam 4. The difference between θ_y and θ_u provides the plastic rotation θ_{pl} , and the difference between θ_y and θ_{max} provides the plastic rotation $\theta_{pl,max}$; by comparing the values for the plastic rotation according to these two definitions (Table 4), the importance of the post-peak branch is clear, especially in the case of Beam 4, for which a double plastic rotation can be attained using this contribution.

The results of the four specimens can be compared and the following conclusion can be drawn:

- the lower rotational capacity of Beam 1 is due to the distribution of the studs because their absence

Table 4 Significant values of the experimental rotations

Beam	M_y (kN·m)	θ_y (mrad)	θ_u (mrad)	θ_{max} (mrad)	$\theta_{pl,u}$ (mrad)	$\theta_{pl,max}$ (mrad)
1	375	13	48	34	35	21
2	375	10	51	38	41	28
3	375	12	52	38	40	36
4	434	15	60	36	45	21

in the central part of the element facilitates local and global buckling.

- the equal rotational capacities of Beam 2 and 3 confirm that the element ductility is independent of the type of slab, i.e., a full slab or slab with profiled sheeting; however, Beam 3 is observed to have a better stability (higher $\theta_{pl,max}$), probably due to the greater number of connectors, which provides a better constraint of the steel profile to the slab and mitigates the global buckling phenomenon.
- the plastic rotation of Beam 4 is approximately 10% higher than that of the other specimens because the descending branch, which was not measured in the other cases, can be used; however, the effect of a higher $(A \cdot f_y)_r / (A \cdot f_y)_a$ ratio, which facilitates local buckling, is evident.

Extending the comparison to the data collected in Table 1, the parameters of Beams 1, 2 and 3 that were used for the tests presented in this study are similar to those of Fabbrocino *et al.* (2001), specimen CB7 of Loh *et al.* (2004) and those of Amadio *et al.* (2004), except for a greater ratio $(\varepsilon_u / \varepsilon_y)_r$, which was not used due to the premature onset of buckling. In all of these other tests, the plastic rotation was greater than that reached in these tests, but the profiles that were used for the specimens of the other authors were less sensitive to local buckling, due to the shape of the profile or the addition of longitudinal stiffeners.

In Fig. 10, an example of the load-strain curves that were detected by the strain-gauges is reported for Beam 1 along the height of the cross-section 50 mm from the mid-span. Therein, in the graph, the position of each strain-gauge with respect to the steel flange in compression is indicated. The graph shows that the strain-gauges that were positioned at the bottom of the profile in the tensile component exhibited a linear trend until yielding; instead, the strain gauges that were placed at the top of the profile in compression resulted in nonlinear behaviour at a load value just below that of yielding, indicating the onset of buckling. Even in Beams 2, 3 and 4, similar deformation patterns were measured.

The local buckling phenomena indicated by the strain gauges in compression together with the global torsion observed along the entire beam indicate that buckling occurred prematurely for the type of section used, probably due to the lack of torsional constraints on the steel cross-section in the support zone and the sensitivity of the used steel profile to distortional buckling; however, a consistent plastic rotation was observed, which can be assumed to be minimal in the beam because it can certainly be increased by suitable constraints in a real frame (i.e., transversal beam and continuity of the beam at the points of zero moment).

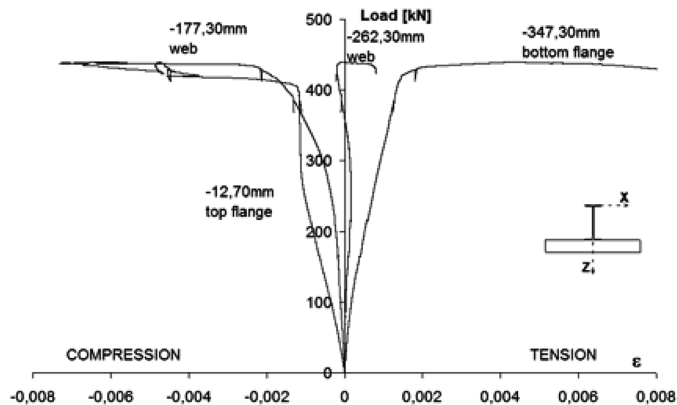


Fig. 10 Strains along the profile height of Beam 1 in the section 50 mm from the mid-span

Table 5 Comparison between the theoretical plastic moments and maximum experimental ones

	x_{pl} (mm)	M_{pl} (kN·m)	M_{exp} (kN·m)
Beam 1	236	484	440
Beam 2	236	484	451
Beam 3	236	484	458
Beam 4	268	529	494

4. First theoretical analysis

The value of the theoretical plastic moment of the cross-section was estimated by neglecting “the moment due to the selfweight of the beam,” the contribution of the tensile concrete strength and the hardening of the steel and by introducing the experimental average value of the yield strength of the profile and bars; the results are depicted in Table 5 and are compared to the maximum experimental moment. It is worth noting that the theoretical values are always greater than the experimental ones, partially due to the model of perfect plasticity in the theoretical implementation, although probably confirming the occurrence of a buckling phenomenon that has prevented the exploitation of the full resources of the materials in hardening; the experimental maximum moment of Beam 1 is lower than that of Beam 2, due to the lower degree of connection of the first beam with respect to the second one.

The moment-curvature relationship was also implemented for the specimens using the experimental characteristics of the materials and by adopting the Bernuolli hypothesis of a plain strain distribution along the composite section.

The steel’s constitutive laws ϵ were assumed to be elasto-plastic with a plateau until a deformation ϵ of 5%. Next, linear hardening was introduced, and the tensile strength of the concrete was neglected such that the slab contribution consisted of only that of the steel bars.

Using the moment-curvature relationship, the deformations along the height of the cross-section for each value of the moment could be assessed. Fig. 11 compares the experimental results and theoretical values for Beam 1 in terms of the strains along a section that was placed 350 mm from the mid-span at various load levels. In the graphs, the reference for the strain positions is the top of the beam in

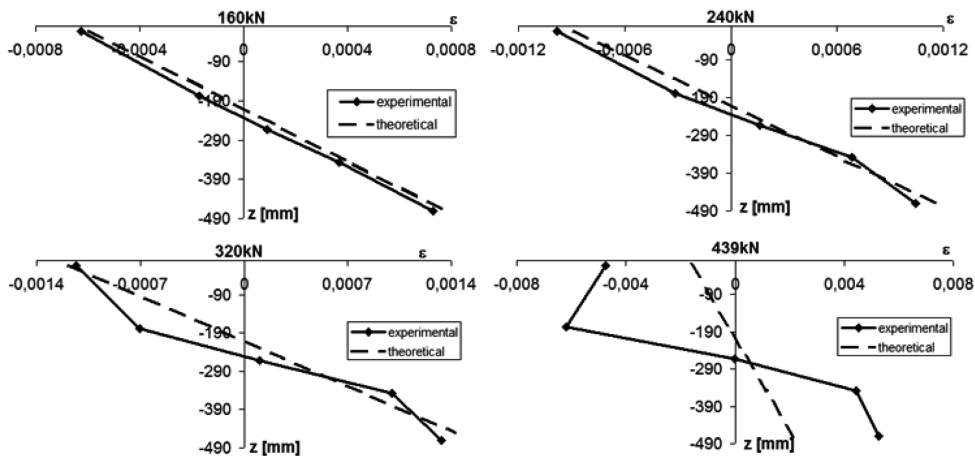


Fig. 11 Strains trend along the cross-section at 350 mm from the mid-span of Beam 1

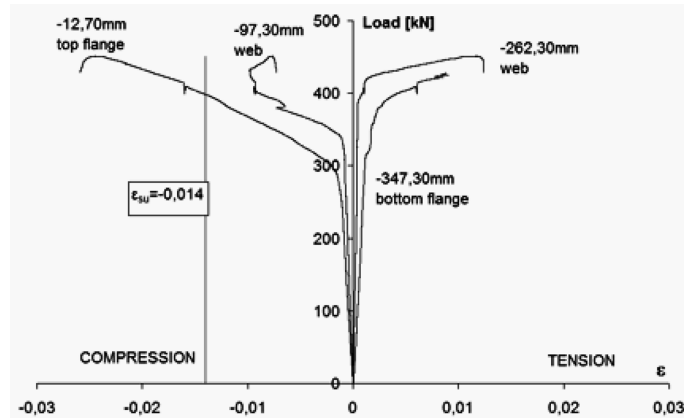


Fig. 12 Comparison of strains in the compression flange recorded in the cross-section at a distance of 50 mm from the mid-span of Beam 2

compression. The last strain at the bottom is the one measured on the steel bars in the slab.

The theoretical-experimental comparison at low load levels (up to approximately 240 kN) shows good agreement between the two results, confirming the effectiveness of the Bernoulli hypothesis for the steel profile and reinforcing bars in the composite beams and the effectiveness of the entire slab.

Interestingly, at higher load levels, the experimental strains deviate from the theoretical values (Fig. 11), showing much higher values, which no longer follow a linear trend; this analysis reconfirms the onset of buckling phenomena.

Comparisons between the theoretical and experimental strains in Beams 2, 3 and 4, which are not reported in this study, provide results that are similar to those for Beam 1.

Another confirmation of premature buckling was obtained by calculating the limit strain ϵ_{su} proposed by Chen and Jia (Eq. (2)) and reported in paragraph 2 and comparing it with the strains reached in compression. The theoretical value of the limit strain of 0.014 was widely exceeded in the tested beams, as reflected in the graph depicted in Fig. 12, where it is compared to the strains of the flange in compression that were recorded on the cross-section 50 mm away from the centre line of Beam 2. Moreover, the limit strain was approximately reached at the yielding point of the flange in tension.

Finally, in Table 6, the experimental plastic rotations of the tested beams are compared to those calculated ($\theta_{pl,t}$) by the formula proposed in [30] and reported in paragraph 2 of this paper. The theoretical values are safer than the experimental values; the values were calculated by considering the descending branch of the force-displacement relationship ($\theta_{pl,u}$), as shown in Table 4; however, if the experimental plastic rotation is recalculated assuming the ultimate rotation at the maximum load

Table 6 Comparison between experimental plastic rotations and theoretical values

	R	ϵ_{su}	y_s	Φ_θ	L_p	$\theta_{pl,t[30]}$	$\theta_{pl,u} / \theta_{pl,t}$	$\theta_{pl,max} / \theta_{pl,t}$
	(-)	(-)	(mrad)	($10^{-6}/m$)	(mm)	(mrad)	(-)	(-)
Beam 1	0,17	0,014	236	9,4	612	30	1,17	0,70
Beam 2	0,17	0,014	236	9,4	612	30	1,37	0,93
Beam 3	0,17	0,014	236	9,4	612	30	1,33	1,20
Beam 4	0,17	0,014	268	5,1	612	28	1,61	0,75

($\theta_{pl,max}$), better agreement with the formulation provisions is revealed, although these values are not always safe (Table 6).

5. Conclusions

The data collected from the technical literature regarding the parameters that influence the rotational capacity of composite beams are not sufficient to tailor specific provisions to their nonlinear performance; however, they confirm that the connection and the steel reinforcement (i.e., the slab) make a difference with respect to the rules governing a bare steel profile. Furthermore, the tests that were carried out on composite frames or more complex composite structures involve more components in the development of post-elastic deformation, making it difficult to clearly extrapolate the beams' contributions. Therefore, additional and more systematic experimental tests on simple beams are required to delineate better the contribution of the various parameters involved; therefore, the results presented in this study can be considered an additional contribution to this topic.

The analysis of the experimental results developed by the authors show that the designed beams and the applied load pattern played an important role in the global and local buckling of the steel profile, despite the presence of the concrete slab. In particular, the test setup reproduces the unfavourable restraint condition of the beam in the frame such that the observed rotational capacity is the minimum value for an actual situation.

Despite the premature onset of local and global buckling, the details of the results and first theoretical comparison suggest that consistent plastic rotation of at least 35-40 mrad was attained. The same applies for the section in Class 2 if the descending branch of the load-displacement curve is used; however, these values are reduced to approximately 20-35 if the curve is stopped at the maximum load. In this last case, a lower plastic rotation is attained for the beam with the partial connection degree and the beam in Class 2 because both circumstances favour buckling phenomena.

The rule proposed by Chen and Jia (2008) for evaluating plastic rotation and limit strain under local buckling is in good agreement with the experimentally determined values, and it is always safe if the load reduction is accepted.

The analysis of the results is underway and is focused on the development of a numerical model that takes into account steel buckling so as to identify, in detail, the structural features that influence the behaviour and may govern the nonlinear performance of composite frames under seismic action.

Acknowledgments

This work was performed under the research project RELUIS-DPC 2005-2008 Line No.5 - "Development of innovative approaches for the design of steel structures and composite steel-concrete."

References

Amadio, C., Fedrigo, C., Fragiaco, M. and Macorini, L. (2004), "Experimental evaluation of effective width in steel-concrete composite beams", *J. Constr. Steel. Res.*, **60**(2), 199-220.

- Aribert, J.-M., Ciutina, A.L. and Dubina, D. (2004), "Seismic response of composite structures including actual behaviour of beam-to-column joints", *Proceedings of the 5th Conference on Composite Construction in Steel and Concrete*, ASCE: Kruger National Park, South Africa, July.
- Chen, S. and Jia, Y. (2008), "Required and available moment redistribution of continuous steel- concrete composite beams" *J. Constr. Steel. Res.*, **64**(2), 167-175.
- DM 14 Genuary. (2008), Min. LL. PP, "*Norme Tecniche per le Costruzioni (NTC)*", Gazzetta Ufficiale della Repubblica Italiana, 29, Italian code in Italian.
- Elghazouli, A.Y., Castro, J.M. and Izzuddin, B.A. (2008), "Seismic performance of composite moment-resisting frames", *Eng. Struct.*, **30**(7), 1802-1819.
- El-Tawil, S., Vidarsson, E., Mikesell, T. and Kunnath, S.K. (1999), "Inelastic behavior and design of steel panel zones", *J. Struct. Eng.*, **125**(2), ASCE.
- Eurocode 3. (2004), "*Design of composite steel and concrete structures. Part 1.1: General rules and rules for buildings*", European Committee for Standardisation, Brussels, Belgium.
- Eurocode 4. (2004), "*Design of composite steel and concrete structures – Part 1.1: General rules and rules for buildings*", ENV 1994-1.
- Eurocode 8. (2004), "*Design provisions for earthquake resistance of structures. Part 1.3: General rules. Specific rules for various materials and elements*", European Committee for Standardisation, Brussels, Belgium.
- Fabbrocino, G., Manfredi, G. and Cosenza, E. (2001), "Ductility of composite beams under negative bending: an equivalence index for reinforcing steel classification", *J. Constr. Steel. Res.*, **57**(2), 185-202.
- Kemp, A.R. (1985), "Interaction of Plastic local and Lateral Buckling" *J. Struct. Eng.*, ASCE, **111**(10), 2181-2196.
- Kemp, A.R., Dekker, N.W. and Trincherro, E. (1995), "Differences in inelastic properties of steel and composite beams", *J. Constr. Steel. Res.*, **34**(2-3), 161-185.
- Kemp, A.R. and Nethercot, D.A. (2001), "Required and available rotations in composite beams with semi-rigid connections", *J. Constr. Steel. Res.*, **57**(4), 375-400.
- Leon, R.T. (1998), "Analysis and design problems for PR composite flames subjected to seismic loads", *Eng. Struct.*, **20**(4-6), 364-371.
- Loh, H.Y., Uy, B. and Bradford, M.A. (2004), "The effects of partial shear connection in the negative moment regions of composite beams, Part I - Experimental study", *J. Constr. Steel. Res.*, **60**(6), 897-919.
- Nie, J., Fan, J. and Cai, C.S. (2008), "Experimental study of partially shear-connected composite beams with profiled sheeting", *Eng. Struct.*, **30**(1), 1-12.
- Providakis, C.P. (2008), "Pushover analysis of base-isolated steel-concrete composite structures under near-fault excitations", *Soil. Dyn. Earthq. Eng.*, **28**, 293-304.